

Theory of complex fluids in the warm-dense-matter regime, and application to an unusual phase-transition in liquid carbon.

M.W.C. Dharma-wardana¹

¹*National Research Council of Canada, Ottawa, Canada, K1A 0R6 **

(Dated: November 26, 2021)

Data from recent laser-shock experiments, density-functional theory (DFT) with molecular-dynamics (MD), and path-integral Monte Carlo (PIMC) simulations on carbon are compared with predictions from the neutral-pseudo-atom (NPA)+ hyper-netted-chain (HNC) approach for carbon, a complex liquid in the warm-dense matter regime. The NPA results are in good agreement, not only with high-density regimes that have been studied via PIMC, but even at low densities and low temperatures where transient covalent bonding dominates ionic correlations. Thus the ‘pre-peak’ due to the C-C bond at $\sim 1.4\text{-}1.6$ Å and other features found in the pair-distribution function from DFT+MD simulations at 0.86 eV and 3.7 g/cm³ etc., are recovered accurately in the NPA+HNC calculations. Such C-C bonding peaks have not been captured via average-atom ion-sphere (IS) models. Evidence for an unusual liquid \rightarrow vapor and metal \rightarrow semi-metal transition occurring simultaneously is presented. Here a strongly correlated metallic-liquid with transient C-C bonds, i.e., carbon at density ~ 1.0 g/cm³ and mean ionization $Z = 4$ transits abruptly to a disordered mono-atomic vapour at 7 eV, with $Z \simeq 3$. Other cases where Z drops abruptly are also noted. The nature of Z , its discontinuities, and the role of exchange-correlation, are reviewed. The limitations of IS models in capturing the physics of transient covalent bonding in warm dense matter are discussed.

PACS numbers: 62.50.-p, 52.25.Fi, 81.05.U- , 78.70.Ck

I. INTRODUCTION.

A number of light elements like hydrogen, boron, carbon, nitrogen, silicon, phosphorous, etc., and their mixtures form strong covalent bonds in the solid and retain much of this bonding, even when molten [1–3] and in warm-dense-matter (WDM) regimes [4–7]. A theory for predicting the properties of these elements and their mixtures reliably and rapidly is needed in many technological applications. Their properties under higher compressions and temperatures are also of great interest in astrophysics [8–10]. Carbon is an important component of inter-stellar matter, white dwarfs, solar and extra-solar planets. WDM carbon is basic to many technologies and inertial-confinement fusion (ICF) ablaters [11, 12].

Many applications require the equation of state (EOS) and transport properties in experimentally inaccessible regimes. The experiments when feasible are quite demanding [6, 13]. The theoretical prediction requires the electronic and ionic structure factors, and their interaction potentials. At low temperatures (compared to the Fermi energy E_F), numerically expensive density-functional theory (DFT) calculations coupled to molecular-dynamics (MD) provide a reliable method if sufficiently large calculations can be made using suitable exchange-correlation (XC) functionals. In DFT the WDM is modeled by a sequence of quenched N -atom periodic crystals thermally evolved using MD. The spurious electronic band structure of each crystal is averaged over the many ionic configurations obtained from MD. Thus

DFT+MD is impractical at higher-temperatures (T) due to the many electronic states needed. At high T and high density ($\bar{\rho}$) path-integral Monte Carlo (PIMC) methods are available for small- N (e.g, 24 atoms) simulations [10].

Since the number of ions N in DFT simulations is limited, other methods are used, especially for ambient-temperature applications. Semi-empirical methods developed from the “embedded-atom” approach have led to “reactive-potentials” which include bonding, dependence on coordination, torsion and bond angle. Carbon is a complex liquid where conjugated bonds ($sp3$, $sp2$, sp) and weak graphite-like partial conjugation occur deploying four valance electrons, i.e. with mean ionization $Z=4$. The Brenner potentials incorporate conjugation and were used by Glosli *et al.*, [2] in their study of the phase transition in liquid carbon. The modern bond-order potentials (LRBOP) by Los *et al.* [14, 15] include long-range effects and are fitted to a very wide data base. However, after applying LRBOP to calculate $S(k)$ of liquid C at 0.52 eV, Kraus *et al.* [6] stated that “this potential appears to be too stiff. Compared to DFT+MD, we find a higher pressure and a more pronounced structure which is not found in the experiment”. Thus LRBOP is hardly promising for $T \sim E_F$ typical of WDM since $T=0.52$ eV, $T/E_F = 0.017$, defines a very low- T WDM where it is already inadequate.

Here we use a first-principles DFT approach treating electrons with a one-body density $n(r)$, and ions with a one-body density $\rho(r)$ to present results using the neutral-pseudo-atom (NPA) model. This couples one-body Kohn-Sham calculations and its electron-ion potentials to pair-distribution functions (PDFs) via integral equations like the hyper-netted-chain (HNC) equation, or MD simulations. NPA+HNC closely recovers

* Email address: chandre.dharma-wardana@nrc-cnrc.gc.ca

PIMC results, and DFT+MD results including C-C covalent bonding signatures in the ion-ion PDFs at low $-T$, but extends seamlessly to high T regimes inaccessible by DFT+MD. In Sec. IV we present evidence for a phase transition of highly-correlated liquid carbon containing transient C-C bonds into a weakly correlated mono-atomic carbon gas. The pressure, compressibility and conductivity in the neighborhood of the transition are presented. The nature of the mean ionization Z , its behaviour near the transition, and comparisons of the NPA+HNC method with PIMC and DFT+MD are given. An appendix discusses details of the electronic structure near the phase transition, and the nature and constraints on the mean ionization Z .

II. THE NEUTRAL-PSEUDO-ATOM MODEL IN THE CONTEXT OF COMPLEX FLUIDS.

Here we demonstrate that the NPA approach [16–19] works sufficiently well for complex liquids in their *metallic phase*, even near the melting point, as already claimed by the present author and Perrot in 1990 [4] by comparing NPA-type calculations with DFT+MD calculations of Galli *et al.* [1] for carbon. There are two types of atom-in-plasma models, viz., Ion-Sphere (IS) models, e.g., [20–22], and the Correlation-Sphere (CS) model used by Perrot and Dharma-wardana, as well as some possible intermediate models. We show that the NPA model used here captures the C-C bonding effects not captured so far in IS models of various sorts, as explicitly stated by, e.g., Starrett *et al.* [23]. Furthermore, we discuss the evaluation of the mean electron density per ion, viz., Z since Blenski *et al.* [24, 25] and Stern *et al.* [26] have pointed out difficulties in their models in defining Z .

In NPA a nucleus of charge Z_n is immersed in its electron distribution $n(r)$ and the corresponding ion distribution $\rho(r)$, where each ‘field’ ion carries its shell of bound electrons compactly contained within their Wigner-Seitz (WS) spheres. The mean electron- and ion- densities become \bar{n} and $\bar{\rho}$ far away from the nucleus, say at $r \geq R_c$. This is taken as the radius of the ‘correlation sphere’ (CS) which is large enough to be an effective ‘infinite volume’. Defining the Wigner-Seitz radius $r_{ws} = (3/4\pi\bar{\rho})^{1/3}$ of the ions, we use $R_c \sim 10r_{ws}$ for strongly coupled systems, while $R_c \sim 5r_{ws}$ may be enough for weakly coupled systems, e.g., at high T . The IS model is obtained if R_c is curtailed to r_{ws} . The Kohn-Sham and HNC equations are solved within this large CS. The R_c plays the role of the linear dimension of the DFT+MD simulation box. However, in DFT+MD, if $N \sim 100$, the equivalent linear dimension is $\simeq 2.3r_{ws}$, while the $R_c \simeq 10r_{ws}$ in the NPA+HNC mimics a 1000-atom volume.

DFT asserts that the free energy $F([n], [\rho])$ is a functional of the *one-body* electron density $n(r)$, and the *one-body* ion density $\rho(r)$, irrespective of complex interactions (e.g., superconductive associations for electrons), and complex-bonding among ions. DFT constructs non-

interacting ‘Kohn-Sham electrons’ that move in the one-body Kohn-Sham potential, and similarly there are non-interacting ‘Kohn-Sham’ ions moving in the ‘potential of mean-force’ $V_m(r)$. The latter is the classical DFT potential acting on an ion, well known in the theory of classical fluids. The variational problem invokes a *coupled pair* of DFT equations [27].

$$\delta\Omega([n], [\rho])/\delta n = 0 \quad (1)$$

$$\delta\Omega([n], [\rho])/\delta\rho = 0 \quad (2)$$

The functional derivatives of the grand potential Ω are implied. The first equation leads to a Kohn-Sham equation which invokes an exchange-correlation functional $F_{xc}^{ee}(n)$ for the electrons in the potential created by the ions, while the second variationally determines the DFT-ion distribution $\rho(\vec{r})$ and invokes an ion-ion correlation functional $F_c^{ii}(\rho)$. The ions, screened by the electron distribution are classical particles without exchange (see Eq. 1.13, p 628 Ref. 28). The equations (1), (2) are connected by a Lagrange multiplier Z enforcing the charge neutrality of the system, $\bar{n} = Z\bar{\rho}$, as in Ref. [27]. Note that both $F_{xc}^{ee}(n, \rho)$ and $F_c^{ii}(n, \rho)$ contain cross terms of the form $F_{xc}^{ei}(n, \rho)$ arising from the electron-ion contribution to the grand potential, viz., $\Omega_{ei}(n, \rho)$. These are discussed by Dharma-wardana in Ref. [28], by Chihara [29], and by Furutani *et al.* [30].

The usual DFT+MD codes do not use Eq. 2, or an $F_c^{ii}([\rho])$ since the positions of the N ions are explicitly in the simulation and held fixed by invoking the Born-Oppenheimer approximation (BOA). The BOA is not needed in the NPA. The use of $\rho(r)$ leads to major simplifications since, instead of having an N -center problem, we have a one-body problem which can be reduced to a ‘single-ion problem’. But the multi-ion correlations captured by the N -ion problem have to be picked up via the $F_c^{ii}[\rho]$. Given the F_c^{ii} , this finite- T ‘average-atom’ defined by Eqs. (1), (2) is a formally exact DFT concept extending the usual Kohn-Sham formalism. Approximations arise in formulating F_{xc}^{ee} for electrons, and in constructing F_c^{ii} for ions. In Refs. [27, 28] F_c^{ii} was shown to be a sum of hyper-netted-chain (HNC) + bridge diagrams and this is known as the MHNC model used here when appropriate. Given m species of ions, e.g., several ionization states, or molecule formation, then a matrix of such correlation functionals $F_c^{ij}(\rho_1, \dots, \rho_m)$ are needed as in multi-component HNC theory [19].

We use a one-component treatment here since the complex fluids studied are in a regime where *no stable* molecules are formed, while transient molecules may be formed. Spherical symmetry around any nucleus is assumed, as appropriate for a fluid WDM, while the method can also be used for solids [31, 32]. The optional assumption of radial symmetry gains simplicity while sacrificing lattice-like information important only at very low- T . Another useful step is to decouple Eq. 1 and Eq. 2 instead of the concurrent solution used in Ref. 27. A simple approximation to the ion distribution $\rho(r)$ is taken to be a ‘spherical cavity’ of radius $r = r_{ws}$ with

$\rho = \bar{\rho}$ for $r > r_{ws}$. Here $r_{ws} = (3/4\pi\bar{\rho})^{1/3}$ is the Wigner-Seitz (WS) radius of the ions. Unlike in most other AA models, this cavity-like ion distribution is a calculational device whose effect will be subtracted out. The cavity with the nucleus at its center creates an object with net zero charge i.e., a weak scatterer. The effect of the WS-cavity in $\rho(r)$ on the electron subsystem of density \bar{n} is assumed to be given by finite- T linear response theory.

The above approximations are justified for the low Z_n elements where the bound-electron core of radius r_c is compactly contained in the WS-sphere with $r_c < r_{ws}$, unambiguously defining the number of bound electrons n_b and an effective ionic charge $Z = Z_n - n_b$. The number of bound electrons is calculated from the Fermi occupation factors $f_{nl}(\epsilon_{nl}, T)$ of the Kohn-Sham bound states (quantum numbers n, l), with eigenvalues $\epsilon_{nl} < 0$. Kohn-Sham theory uses a *homogeneous* non-interacting distribution of electrons at the interacting density \bar{n} as the reference state, and the chemical potential is the non-interacting value μ^0 , while $f_{nl} = 1/[1 + \exp\{(\epsilon_{nl} - \mu^0)/T\}]$. In the NPA, the plasma outside the correlation sphere ($r > R_c$) is bulk-like. Unlike in ion-sphere models, the Kohn-Sham potential for $r > R_c$ is the NPA reference zero potential (see Eq. 2.11 of Ref. [27]); hence the effective μ is simply μ^0 . The Z defined via the bound states is

$$Z = Z_b = Z - n_b; \quad n_b = \sum_{nl} 2(2l+1) \int d\vec{r} f_{nl} |\phi_{nl}(r)|^2 \quad (3)$$

Here $\phi_{nl}(r)$ is a bound-state (i.e., $\epsilon_{nl} < 0$) solution of the Kohn-Sham equation.

The NPA model satisfies the finite- T Friedel sum rule which applies to the plane-wave like continuum states $\psi_{kl}(r)$, $\epsilon_k = k^2/2$ and having phase shifts $\delta_l(k)$.

$$Z = Z_F = \frac{2}{\pi T} \int_0^\infty k f(\epsilon_k) \{1 - f(\epsilon_k)\} \sum_l (2l+1) \delta_l(k) dk \quad (4)$$

Thus we see that the Kohn-Sham solution for the bound and continuous spectra, and Z are tightly controlled by the Friedel sum rule, the f -sum rule, and charge neutrality. Charge neutrality implies that

$$Z = Z_{cn} = \bar{n}/\bar{\rho} = (4\pi/3)\bar{n}r_{ws}^3 \quad (5)$$

We need $Z = Z_b = Z_F = Z_{cn}$ at self-consistency. The NPA consists of the nucleus surrounded by its electron distribution $n(r)$ and the input ion distribution $\rho(r)$ extending up to $r = R_c$ forming a neutral object. The presence of the cavity (or $\rho(r)$) makes the net NPA charge to be zero, and the Friedel sum is zero precisely for that WS-cavity whose charge $Z_{cn} = Z$. Hence a trial electron density \bar{n} is input and the ion density $\bar{\rho}$ (i.e., cavity radius r_{ws}) which self-consistently satisfies the neutrality and sum rules etc., is calculated. That \bar{n} which yields the required physical ρ is determined iteratively.

Note that $n(r)$ extends over the whole correlation sphere $r = R_c$, and not limited to the WS-sphere, $r = r_{ws}$

as used in many ‘atom-in-plasma’ (AIP) models. Furthermore, such AIP models where the ‘pseudo-ion’ is restricted to an ion sphere do not have a Friedel sum rule, and cannot use the non-interacting μ^0 as required by DFT. This is discussed more fully in Sec II C.

The so-called ‘Chihara decomposition’ separating bound and free spectra of an ion, invoked in expressing one-atom properties, e.g., in the ‘ion-feature’ needed for X-ray Thomson scattering (XRTS) theory [33], occurs naturally in the NPA. However, the Kohn-Sham states do not correspond to the physical one-particle states of the electrons. They are given by the corresponding Dyson equation [34]. Although the NPA is not a physical object, it is a rigorous DFT construct. The NPA becomes thermodynamically variational when it is coupled with Eq. (2).

A. Calculation of pair-potentials and the ion distribution $\rho(r)$.

In most cases the above simplifications leading to the NPA hold, and the electron distribution $n(r)$ around a nucleus in the simplified ion (i.e., a cavity) distribution is easily calculated from the Kohn-Sham equation. The next step is to solve Eq. (2) for the accurate ion distribution $\rho(r) = \bar{\rho}g_{ii}(r)$ where $g_{ii}(r)$ is the ion-ion PDF. In Ref. [27] we show that solving Eq. (2) is equivalent to solving an HNC-type equation. Thus $\rho(r)$ is evaluated from the ion-ion pair-potential determined entirely by the electron charge density $n(r)$, the input nuclear charge Z_n and temperature T . The electron density $n(r)$ of the NPA is corrected for the presence of the spherical cavity using perturbation theory. Then the resulting $n(r)$ is written in the form:

$$n(r) = n_b(r) + \Delta n_f(r) + \bar{n} \quad (6)$$

This division is unambiguous since the bound density $n_b(r)$ is compactly inside the WS sphere. Since $\bar{n} = Z\bar{\rho}$, and since $\bar{\rho}$ is the given matter density, Z is simply the free-electron density per ion in the plasma. However, some authors have claimed that Z “.does not correspond to any well-defined observable in the sense of quantum mechanics”, i.e., that there is no quantum operator corresponding to Z [25]. Within that view, there is no quantum operator for the temperature or the chemical potential either. We review AIP models of Z and its physical nature in more detail in sec. II C. We subscribe to the standard view that Z is a measurable physical quantity.

The Fourier transform of the cavity-corrected free-electron pileup, viz., $\Delta n_f(k)$ is used to construct an electron-ion pseudopotential $U_{ei}(k)$. We omit various technical details of the NPA model as they have been amply discussed in many publications since the 1970s in applications to $T = 0$ metals, finite- T plasmas, [17–19, 27, 31] and more recently [20, 35, 36] for applications to ultra-fast two-temperature matter. The cavity corrected $\Delta n_f(k)$ is the density modification occurring in

a *uniform* electron gas with a static neutralizing background, arising from an ion of charge Z placed in it. It determines $U_{ei}(k)$ and the ion-ion pair potentials $V_{ii}(k)$, via the fully-interacting static-electron response function $\chi(k, T_e)$. In Hartree atomic units,

$$U_{ei}(k) = \Delta n_f(k)/\chi(k, T_e), \quad (7)$$

$$\chi(k, T_e) = \frac{\chi_0(k, T_e)}{1 - V_k(1 - G_k)\chi_0(k, T_e)}, \quad (8)$$

$$G_k = (1 - \kappa_0/\kappa)(k/k_{\text{TF}}); \quad V_k = 4\pi/k^2, \quad (9)$$

$$k_{\text{TF}} = \{4/(\pi\alpha r_s)\}^{1/2}; \quad \alpha = (4/9\pi)^{1/3}, \quad (10)$$

$$V_{ii}(k) = Z^2 V_k + |U_{ei}(k)|^2 \chi_{ee}(k, T_e). \quad (11)$$

Here χ_0 is the finite- T Lindhard function, V_k is the bare Coulomb potential and G_k is a local-field correction (LFC). The finite- T compressibility sum rule for electrons is satisfied since κ_0 and κ are the non-interacting and interacting electron compressibilities respectively, with κ matched to the $F_{xc}(T)$ used in the Kohn-Sham calculation. In Eq. 10, k_{TF} appearing in the LFC is the Thomas-Fermi wavevector. We use a G_k evaluated at $k \rightarrow 0$ for all k instead of the more general k -dependent form (e.g., Eq. 50 in Ref. [37]) since the k -dispersion in G_k has negligible effect for the WDMs of this study.

Eq. 11 gives the pair-potential to second order in the pseudopotential. Higher order terms can become important, as displayed in Fig. 2 and will be discussed in the context of transient bond formation. In this study where T is high enough to prevent strong bond formation, we use only the second order form. Once the pair-potential $V_{ii}(r)$ is determined, the ion-ion PDF $g_{ii}(r)$ can be determined using a classical MD simulation; or via the MHNC equation coupled to the Ornstein-Zernike (OZ) equation. The later route, viz., NPA+MHNC is numerically very fast but requires a Bridge term $B(r)$ which includes linked multi-ion correlations terms but not those arising from quantum effects like C-C bonding.

$$g(r) = \exp\{-\beta V_{ii}(r) + h(r) - c(r) + B(r)\} \quad (12)$$

$$h(r) = c(r) + \bar{\rho} \int d\vec{r}_1 h(\vec{r} - \vec{r}_1) c(\vec{r}_1) \quad (13)$$

$$h(r) = g(r) - 1. \quad (14)$$

Thermodynamic consistency (e.g., the virial pressure being equal to the thermodynamic pressure) is obtained by using the Lado-Foiles-Ashcroft (LFA) criterion (based on the Bogoliubov bound for the free-energy) for determining $B(r)$ using the hard-sphere model bridge function [38, 39]. That is, the hard-sphere packing fraction η is selected according to an energy minimization that satisfies the LFA criterion. The iterative solution of the MHNC equation, i.e., Eq. (12) and the OZ-equation, Eq. (13), yields a $g_{ii}(r)$ for the ion subsystem. The LFA criterion and the associated hard-sphere approximation can be avoided if desired, by using MD with the pair-potential to generate the $g(r)$.

One may now ask if $\bar{\rho}g(r)$ should be used as the new ion-density profile in Eq. 1 instead of the spherical cavity, as was done in Ref. 27. For all cases studied where

the bound-electron core is compactly contained inside the WS-sphere, such further iterations are unnecessary. If the difference between the cavity profile and the $g(r)$ -profile is used in perturbation theory (or in a Kohn-Sham calculation), the bound state distribution should not change perceptibly, and hence Z remains unchanged. The effect on $\Delta n_f(r)$ can be significant but the pseudopotential $U_{ei}(k)$ remains unchanged for the conditions where a linear pseudopotential holds [35]. This is true since the effect of the ion-density profile is subtracted out before Eqs. (7)-(11) can be applied. The thermodynamic consistency of the model is easily checked by the satisfaction of the compressibility sum rule, viz.,

$$S_{ii}(k \rightarrow 0) = Z\bar{\rho}T\kappa_T, \quad \kappa_T = -\frac{1}{v} \left[\frac{\partial V}{\partial p} \right]_T. \quad (15)$$

Calculations confirm that carbon WDMs satisfy the requirements that enable us to decouple the pair of DFT equations 1, 2 and use the NPA+MHNC mono-atomic equations for carbon WDMs whose $\bar{\rho}, T$ do not allow the formation of *stable* covalent C-C bonds. If such molecular species are formed, then an explicit multi-component NPA+MHNC formulation which includes molecular species, i.e., a neutral-pseudomolecule (NPM) model has to be used. But a molecular model is not needed and we closely recover available DFT+MD and PIMC results for carbon WDMs quite accurately. A comparison of $g(r)$ and the density of states (DOS) from DFT+MD [1] and those of an NPA-like calculation for carbon near the melting point were already presented in 1990 [4].

After such validation of the NPA, we use the method to uncover an unusual phase transition in a somewhat lower-density carbon where there are also only transient C-C bonds. This strongly-correlated carbon fluid at $\simeq 7$ eV undergoes a liquid-to-gas type transition ('boiling' transition) accompanied by a change in the state of ionization Z of the carbon atoms. The reduced ionization removes the electrons needed for C-C bonding and drives the transition. The reduction in the mean free-electron density causes a discontinuity in Z with $\Delta Z \simeq -1$.

B. The free-electron density per ion as an experimentally accessible quantity.

The free-electron density per ion in a plasma, viz., Z , is even claimed to "not correspond to any well-defined observable in the sense of quantum mechanics" by some workers, while some others regard it as a 'subjective, model dependent quantity'. Hence a discussion of Z and a review of its discontinuities are useful.

Unlike in simple quantum mechanics, quantum statistical theory requires an associated heat bath and the introduction of quantities like T , μ , Z , etc., which appear as Lagrange multipliers needed in the theory [27], rather than simple operator mean values. Alternatively, extended Hilbert spaces, thermofield dynamics etc., can

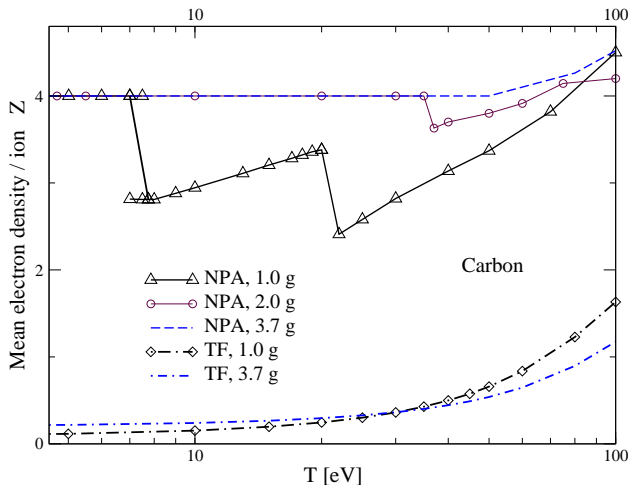


FIG. 1. The average ionization Z of carbon as a function of T for 1-3.7 g/cm³. The ionization given by Thomas-Fermi (TF) theory, More *et al.* [57] is also given. Note the existence of two possible values of Z (hysteresis) from two possible Kohn-Sham solutions near $T=7$ for the density 1.0 g/cm³ at the phase-transition. (see appendix).

be used to give a completely operator-like formulation or a hybrid formulation for these quantities as well. These broader questions are discussed briefly in Chapter 8 of Dharma-wardana [40], and in Heslot [41]. Quantities like Z , i.e., the mean electron density per ion, the chemical potential μ , T , are measurable physical quantities.

Ion-Sphere models confine the electron density $n(r)$ to the Wigner-Seitz sphere, so that $n(r) = \bar{n}$ for $r > r_{ws}$. The Kohn-Sham equation is solved only within the WS-sphere. This results in a number of non-DFT characteristics in IS models. The confinement is equivalent to the addition of a spurious confinement potential $V_{conf}(r)$ via the imposed boundary conditions. Hence V_{conf} may be regarded as a non-local one-body potential. But DFT maps many-body interactions also to such a one-body potential and hence the spurious $V_{conf}(r)$ can technically also correspond to an interacting system. That is, the mapping to a non-interacting *homogeneous* electron system with a chemical potential μ^0 is now replaced by a mapping to an inhomogeneous system with a μ_{conf} chosen so that the electrons inside the WS integrate to Z_n . This model is used in Purgatorio, MUZE etc, but Starette *et al.* [23] and Piron *et al.* [25] have also used it in some of their implementations, though not necessary. Figure 12 of Blenski *et al.* [24] shows electron density oscillations outside the ion-sphere, and yet we are told that the model fails for normal-density Al as $T \rightarrow 0$, perhaps because the cavity is treated as an invariant feature of their model which is not subtracted out. Given that the thermal de Broglie wavelength of electrons is $\lambda_e \propto \sqrt{1/T}$, confinement becomes unphysical as $T \rightarrow 0$. In any case, any such confinement is inconsistent with the free functional variation of $\Omega(n, \rho)$ with $n(r)$ needed in Eq. 1. The non-variational nature of the IS-model was

indeed noted by Blenski *et al.* However, at sufficiently high T , the effect of $V_{conf}(r)$ may be neglected and the IS-approximation becomes valid.

The correlation-sphere model, with $R_c = 10r_{ws}$ used in NPA does not confine the electrons to the WS-sphere but solves the Kohn-Sham equation up to R_c . The central potential plus the neutralizing cavity is a weak scatterer, where the free-electron phase shifts (calculated at the $r \rightarrow R_c$ limit) satisfy the Friedel sum, adding to zero. This procedure breaks down for bound-states which extend outside the WS-sphere. However, this is not the case for the carbon plasmas studied here.

There are several specifications of Z in IS models [20, 26] but no self-consistency exists. Figure 4 of Stern *et al.* [26] display three models of Z , labeled (a) $Z_{continuum}$ which is the total number of unbound ($\epsilon_k > 0$) electrons in the WS-sphere (b) $Z_{background}$, an estimate of the continuum electron density using the ideal DOS, and (c) Z_{ws} , i.e., the free-electron density on the WS-sphere surface, viz., $4\pi(r_{ws})^2 n(r_{ws})/\bar{\rho}$. Since the IS model becomes increasingly valid at high T , two of the estimates, i.e., (b), (c) but not (a), approach each other as $T \rightarrow \infty$, but diverge as $T \rightarrow 0$. According to Blenski *et al.* [24] the $T \rightarrow 0$ estimate of Z for normal-density aluminum obtained from their variational model approaches that of Thomas-Fermi theory (see Fig. 1). Refs. [18, 19] discuss the aluminum EOS and Z via NPA. For normal density Al, the NPA Z equals 3 for $T < E_F$. We do not support the view of Blenski *et al.* [24] that “...all quantum models seem to give unrealistic description of atoms in plasma at low temperature and high plasma densities”.

One may ask what answers are available regarding Z from more detailed simulations, e.g., DFT+MD methods using VASP, ABINIT and such codes. In solid state physics, such codes provide electronic structure data to calculate properties like the complex dielectric function [42, 43], or specific Fermi surface properties. These are used to determine the free-electron density \bar{n} per ion, i.e., Z . Even for a metal like gold where the d -electrons extend outside the WS-sphere, \bar{n} per atom (i.e., Z) contributing to the optical conductivity is found to be unity for $T < 2$ eV, i.e., below the $5d \rightarrow 6s$ threshold, as is also found from optical experiments [44] on gold. Thus the free-electron density per ion is a well-accepted quantity. This view is current even in WDM studies (c.f., Review of XRTS phenomena by Glenzer and Redmer [33]).

Consider the experimental measurement of Z . The plasmon peak positions (Stokes and anti-Stokes values) give a mean value of \bar{n} . Their intensity ratio can be used (assuming detailed balance) to obtain T which is not an operator but the Lagrange parameter associated with the conservation of $\langle H \rangle$ where H is the Hamiltonian. Then, knowing the ion density $\bar{\rho}$ and \bar{n} , we obtain \bar{Z} . This $\bar{n}/\bar{\rho}$ must agree with the \bar{Z} measured independently from the conductivity which is obtained from the absorbed, transmitted and reflected signals of a probe beam yielding the dynamic conductivity $\sigma(\omega)$. The $\omega \rightarrow 0$ limit of $\sigma(\omega)$ yields the static conductiv-

ity and hence Z . The XRTS ion-feature $W(k)$ can be used to obtain another estimate of Z . Hence we have at least three independent measures of Z that the experimentalist obtains using (as far as possible) a single self-consistent theory. Many other experimental measures of Z exist since Z occurs in the ion-electron pseudopotential, but we will not enumerate them here. The NPA approach offers a consistent, parameter-free theory, as demonstrated in Ref. [36] and Ref. [45] for extracting Z from experimental data. DFT+MD is also such a theory, although it does not yield Z directly. Many WDMs and their T , Z and σ have been extracted using DFT+MD, from experiments using femto-second laser probes. Even in space plasmas and discharge-tube plasmas, Z , i.e., the free-electron density per ion, is measured routinely using Langmuir probes, where the potential of the probe is compared to a reference electrode. Hence, while some scientists question the physical admissibility of ‘indirect’ properties like Z , T , we do not subscribe to that view.

C. The nature of the discontinuities in Z .

Fig. 1 reveals many discontinuities in Z as a function of T . We study in detail the discontinuity in Z for $\rho \sim 1$ g/cm³ near $T = 7$ eV and discuss the other discontinuities (e.g. at 22 eV, $\rho = 1.0$ g/cm³) only briefly, leaving their detailed elucidation to future work. The existence of such discontinuities in Z has been well-known and it has been a matter of concern for EOS studies.

The nature of the discontinuities in \bar{Z} in NPA-like models needs to be clarified. The one-atom NPA can be generalized to an N -atom pseudo-molecule (NPM) calculation that becomes analogous to the N -atom quenched-solid model of WDM used in DFT+MD studies via VASP, ABINIT etc. The Z discontinuity problem in NPA becomes in NPM the well-known band-gap problem in the DFT of solids, but now with *partial electron occupations* in bands due to the finite- T Fermi distribution. A limited solution to the band gap problem at $T = 0$ is to use the GW method in a somewhat inconsistent but successful approximation without a vertex correction $\Gamma(\omega)$. In the NPA, such a GW-like implementation based on solutions to the Dyson equation for H-plasmas was given by Perrot and Dharma-wardana in 1984 [34]. An alternative approach, which has not been examined sufficiently by implementations is the use of finite- T ion-electron XC-potentials, self-interaction (SI) corrections etc., which may play a crucial role at these discontinuities. In the case of states which extend beyond the WS-sphere, some authors have tried *ad hoc* approaches using broadening or modifying the Kohn-Sham states. But KS-states cannot carry any broadening as they apply to a *non-interacting* electron gas at the interacting density.

In Fig. 1 we present the mean ionization Z of isochoric carbon at 3.7, 2.0 and 1.0 g/cm³ as a function of T . Fig. 1 indicates sharp *downward* change in Z , both for C at 2.0 g/cm³ and 1.0 g/cm³. Unlike a rise in Z caused by

shell ionization, downward drops are indicative of metal-semimetal transitions. If the bound-electron core of the carbon atom remains compactly within the WS-sphere, and if the three estimates Z_b, Z_F, Z_{cn} defined in Eqs. 3,4, and Eq. 5 fall with 95% of each other, a converged NPA solution and its Z are obtained. The deviations from self-consistency occur due to short-comings in F_{xc}^{ee} which may lack SI corrections and multi-species effects. The ~ 7 eV fluid displays a transition between two ionization species, $Z=3$ and $Z=4$, and even the AA prediction in the local density approximation (LDA), without SI corrections, allows Z to dip to only 2.8 at ~ 7 eV. SI corrections would push Z to 3. We show in Sec. IV that at 7 eV the reduction in Z is accompanied by a loss of ion correlations due to loss of transient C-C bonding in the fluid.

If the Z obtained from the NPA-LDA is a quantity like 2.5, then model of a mixture of ions with integral values of $Z = 2, 3$, and 4 for C (as in Ref. [19] for aluminum) is needed, with an SI-corrected $F_{xc}^{ee}(n, T)$. Such corrections are also in DFT+MD studies of such transitions. Without a SI term, bound states favour double occupancy, while the SI (even a simple Hubbard U model) favours single occupancy. Thus hydrogen-plasma models without SI contain only H⁻ ions, with no H atoms.

Discontinuities at higher T . No C-C bonding effects are likely even at low densities for $T > 8$ eV as $E_{cc} \simeq 8$ eV even in dilute gases. But the discontinuity in Z at 20 eV is very similar to that at 7 eV. The discontinuity in Z at $\sim 20 - 22$ eV for $\rho=1.0$ g/cm³ is at a $\Gamma_{ii} \simeq 2.26$ while $T/E_F \simeq 2.5$, and $Z \sim 2.5$. While there is weak short-range order in the fluid, the main effect is the repopulation of the $2p$ shell of carbon. The conductivity of the fluid calculated using LDA-XC drops, as in a metal-semimetal transition, but with no major change in the structure of the fluid with little ionic correlations. Given a mean $Z = 2.5$, a description as mixture of electrons and ions, $Z_i = 2, 3, 4$, with compositions x_i , with suitable SI corrections applied to the $F_{xc}^{ee}(n, T)$ is necessary to treat this case (as in the case of Al studied in Ref. [19]). Then a modest decrease in the mean Z and the conductivity may probably occur at 21 eV. The slow rise of Z from ~ 2.5 at 22 eV towards 6 involves a redistribution of the composition x_i of ions over the long T -range.

The discontinuity at 35 eV for carbon, $\rho=2.0$ g/cm³ is of the same genre as that for carbon, $\rho=1.0$ g/cm³ at $T=21$ eV. Here too the carbon fluid with $Z \simeq 3.6$ needs a treatment as a mixture of $Z=3$, and $Z=4$ species together with XC-functional including SI, going beyond LDA.

Discontinuities from quasibound states. – Discontinuities in Z arise in LDA average-atom treatments of WDMs, especially in higher- Z_n elements, from bound states emerging as quasi-bound states (QBS) extending beyond r_{ws} . Such QBS need not cause discontinuities in EOS properties due to compensating changes in the DOS, e.g., as determined by the phase-shifts of the continuum states [48]. Several AA-models including that of Starrett and Saumon (SS) [49] use a level-broadening parameter τ to smooth out QBS discontinuities in Z .

As Kohn-Sham levels are eigenstates of ‘non-interacting’ electrons, a level width γ is not available within DFT where the Kohn-Sham states are for non-interacting electrons. If level widths are needed, a Dyson equation has to be solved and the imaginary part of the self-energy provides the level width, as in Ref. [34]. Instead, a *transport* width $1/\tau_{tr}$ obtained from the Ziman equation has been used in several atom-in-plasma models (e.g., see Appendix C of Ref. [49] and references there in). The $1/\tau_{tr}$ is not a level width, and reflects the momentum relaxation of continuum electrons in the $E_F \pm T$ window. The QBS (e.g., d -bands calculated in an AA-model) arise from core-state features lower in energy than the Fermi energy, and $1/\tau_{tr}$ cannot be simply transferred to other bands. In cases where the bound states delocalize beyond the WS-sphere, a multi-center ‘neutral-pseudomolecular’ formulation becomes necessary in DFT as constructing suitable XC-functionals is difficult. Given that valid discontinuities in Z exist, forcing Z and other properties to be smooth across a discontinuity is to obliterate valid physics using an artifice.

D. NPA average ions and covalent bonding.

Many low- Z_n materials, e.g., H, O, N, P, Si and their mixtures show many phases and covalent bonding at low T . Such bonding persists into their WDM states. The C-C bond in its various forms (single, double) has a bond energy E_{CC} of the order of $\sim 4 - 8$ eV. However, in a WDM medium, the presence of free electrons leads to screening effects absent in non-conducting media, making the bonding weaker and transient at higher temperatures $T \sim E_{CC}$. The valance Z of carbon at low T even in nonconducting systems is 4, where three p electrons and one s -electron are available for hybridization. When bonding occurs, $n(r)$ in the region *between* two carbon atoms (i.e., between the two WS-spheres) increases, as easily seen even from the Heitler-London description of bonding (sec. 7.3.2, Ref. [40]) and even from the mid-bond density [50]. A spatial redistribution of valance electrons occurs, but there is no change in $Z = Z_n - n_b$ as the core electrons are not affected; the total number of free-electrons per atom is conserved, and Z remains 4. No gap or pseudogap is found in the DOS near E_F . An NPA-type calculation for the DOS for carbon just above the melting point (transient C-C bonding), and a comparison with the corresponding DFT+MD for the DOS and $g(r)$ of Galli *et al.* have been given in Ref. [4].

When transient bonding occurs, the relevant configurations captured by the AA model of the NPA are an average over the transiently bonded ion configurations. The pair-potential between these average ions is given by Eq. 11. The minima (or turning points) in $V_{ii}(r)$ can produce ‘bonding’ between NPA-carbons, while the principle minimum will usually define a bond having the longest lifetime since the system is in a thermal ensemble. The ion-ion PDFs in the non-bonding regime of densities

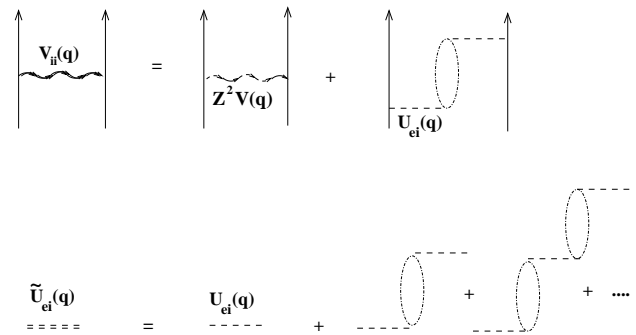


FIG. 2. Vertical arrow represent ion propagators, while the electron-hole interaction $Z^2 V_q$ is converted into the ion-ion pair-potential as in Eq. 11. However, the pseudopotential $U_{ei}(q)$ can be resummed to give $\tilde{U}_{ei}(q) = U_{ei}/\{1 - U_{ei}\chi(q)\}$ and indicates the possibility of new collective modes associated with transient bond-formation in complex liquids.

show peaks due to packing effects. As the bonding region in the phase diagram is approached, a prepeak appears. This is an average over all configurations around a single carbon ion. The bonding peak (‘prepeak’) in $g(r)$ of liquid carbon has been analyzed in such terms by Correa *et al.* [51], Galli *et al.*[1] and by earlier workers as well.

Thus an ‘average dimer’ in DFT is more complex than just two ions bonded together. The ‘effective bond’ that determines, say the first peak in $g(r)$ is an average over sp^3 , sp^2 , sp configurations with one or many neighbors. Even higher coordinations may occur at high compression. In the NPA picture the shells of neighbours around an ion depend on the interplay of many minima in the Friedel oscillations in the ion-ion pair potentials, mean-field effects and ion-correlation effects all contributing to the potential of mean force acting on a field ion. At very low T , the highly correlated C-C bonded forms of the liquid become increasingly favored, while at high T the monomer-fluid (i.e., single ions) becomes dominant. Thus, under favourable circumstances, a ‘dimer-monomer’ phase-transition can be anticipated as T is increased. The valance electrons DOS modifies in forming a transient band of bonding states and anti-bonding states, but the mean charge Z (i.e., valance) does not change during bond-formation. An increase of T leads to less screening and an increased nuclear attraction on electrons, binding them, decreasing Z . The available free electrons decrease and bonding decreases. Hence such ‘dimer-monomer’ transitions occur near a *decrease* in Z .

The form of the pair-potentials implies that even the simplest NPA approach implicitly allows a mixture of two fluids. This view is theoretically equivalent to Straüssler and Kittel’s [52] ‘pseudo-binary mixture’ model basic to the theory of complex fluids. In Ref. 4 Dharmawardana and Perrot showed that the ionic-structure of liquid-metal phases of C, Si and Ge (which show unusual shoulders at the mean peak) can be obtained using an NPA-like approach. A more recent discussion for WDM-

Si is given in Ref. 35. The electrons form transient bonds, and become “heavy” due to self-energy corrections accruing to the electron propagators, specially near $2k_F$. This Fermi-liquid model quantitatively explained the unusual $S(k)$ of Si and Ge, viz., the shoulder on the high- k side of the main peak [4, 35] without invoking chemical bonds “captured” in computer simulations [1]. In the present case the formation of time-dependent networks of C-C bonds can be understood as in Fig. 2. Neglecting vertex corrections and ladder contributions, an all-order interaction that extends over the liquid can be given as:

$$\tilde{U}_{ei}(q) = U_{ei}(q)/\{1 - U_{ei}(q)\chi(q)\} \quad (16)$$

The poles of $\tilde{U}_{ei}(q)$ signal the appearance of new elementary excitations in the liquid. The second-order form becomes valid only for sufficiently high T compared to the average energy of the C-C bonds, as is the case for the 7 eV fluid studied here. The C-C bonded ion-excitation is a break-off mode of the ion-optic folding of the ion-acoustic mode leading to complete localization in the ladder-diagram limit (not shown in the figure). The pole-structure of Eq. 16 shows that transient C-C bond formation is a true collective phenomenon in complex conducting liquids. Computer-simulation ‘snapshots’ of quenched configurations cannot capture its essentially dynamic Fermi-liquid character.

III. COMPARISONS WITH DFT+MD RESULTS, AND PIMC SIMULATIONS.

The applicability of the NPA for complex liquids was proposed back in 1990 [4], but few DFT+MD calculations or experiments for WDMs existed to validate the NPA by detailed comparisons. Currently there are several DFT+MD calculations, path integral Monte Carlo (PIMC) results, and experiments; we use them to compare the NPA calculations in this section.

A. Carbon at 3.7 g/cm³ and at ~100GPa.

Experiments and DFT+MD are available for carbon at a density of 3.7 g/cm³, $T \simeq 0.52$ eV (6,000K) and 0.86 eV (10,000K), with the pressure within 100-200 GPa. The mean ionic charge Z remains 4.0 even beyond 50 eV while E_F is 29.9 eV. Thus WDM carbon probed by Kraus *et al.* [6] at 6,000K and 10,000K is such that $\theta = T/E_F < 0.03$. Hence the use of $T = 0$ XC-functionals and standard DFT+MD is justified. Kraus *et al.* report the $S(k)$ obtained from their simulations, while Whitley *et al.* [5] have published $g(r)$ data for an overlapping regime. We use these results and the PIMC predictions [10] to benchmark the NPA method against DFT+MD as well as PIMC methods.

An all-electron Kohn-Sham calculation for a carbon nucleus immersed in an electron fluid (with $\bar{n} = 0.1099$

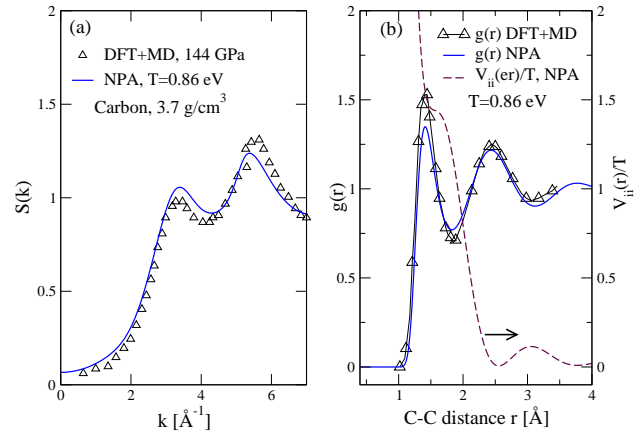


FIG. 3. (a) Comparison of the $S(k)$ of liquid carbon from the NPA+HNC with the DFT+MD (GGA) simulation reported by Kraus *et al.* [6] at 0.86 eV and 3.7g/cm³. (b) The corresponding NPA C-C potential (in units of T), the $g(r)$ from the NPA, and the DFT+MD $g(r)$ of Whitley *et al.* [5].

electrons per a.u. of volume when the carbon density is 3.7 g/cm³) inside a correlation sphere of radius of 10 r_{ws} was used to construct the neutral pseudo atom. The Wigner-Seitz radius is 2.0558 a.u. The free-electron pile-up $\Delta n_f(k)$ around the carbon nucleus defines $U_{ei}(k)$, and $V_{ii}(k)$, i.e., Eq. 11. The ion-ion structure factor $S(k)$ is calculated using the HNC equation and not the MHNC for reasons discussed below. The pair potential, $g(r)$ and $S(k)$ for carbon at 3.7 g/cm³, $T = 0.86$ eV are displayed in Fig. 3. Here the ion-ion coupling constant $\Gamma_{ii} = Z^2/(r_{ws}T) \simeq 246$ and hence we have a strongly coupled fluid. Even with strong coupling, it is clear from Fig. 3 panel (a) that the NPA+HNC calculation matches the DFT+MD calculation quite closely.

The physical meaning of the peaks becomes clear by considering $S(k)$, and $g(r)$. In normal liquids (e.g., liquid Aluminum at low T [47]), the first peak in $g(r)$ occurs near 1.6-1.7 times r_{ws} (see Fig. 4); whereas here the first peak is $\simeq 1.3r_{ws}$, i.e., a short-range ‘prepeak’ occurs earlier than the main peak of simple dense fluids.

Such short-range correlations (large- k) involve bond formation and local order. The hard-sphere bridge term was not designed for such bonding effects, and hence HNC is used rather than the MHNC. This slightly underestimates the peak height, while the peak positions are within $\sim 5\%$ of the DFT+MD peaks. The position of the first peak (~ 1.4 Å) in $g(r)$ corresponds to a typical conjugated C-C bond distance. From panel (b) of the figure we see that the C-C bond formation corresponds to a stationary point in V_{ii} with a *positive* energy.

Some readers may wonder if the turning point at a *positive* energy in $V_{ii}(r)$ can be the cause of the first peak in $g(r)$. As cited in our 1990 study of carbon [4], this feature is familiar from the $g(r)$ and the pair-potential of liquid aluminum (see pair-potentials given in Ref. [4, 32]) and other high- Z liquids. While the high-density electron fluid attempts to push the ions inwards to become dense

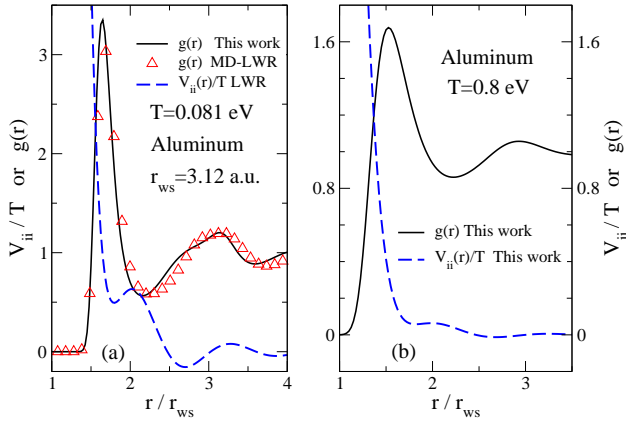


FIG. 4. (a) The pair-potential and $g(r)$ from the MD simulation of normal-density Al at its melting point (0.081 eV) by Levesque-Weiss-Reatto (MD-LWR) [54] compared with our calculation. The main peak is near the *positive* energy stationary point in the potential. The $g(r)$ peaks roughly correspond to the Friedel minima in the potential, and phase out for larger r . (b) The corresponding $g(r)$ and pairpotential at a higher T , 0.8 eV, where the positive stationary point in $V_{ii}(r)$ locates the main peak in $g(r)$, as in Fig. 3(b).

and gain the higher XC-energy of the Gellman-Breuckner limit, the ions repel each other, and even the innermost inflection point in $V_{ii}(r)$ becomes the best compromise. The MD simulations for liquid aluminum near its melting point using the Dagens-Rasolt-Taylor potential for aluminum by Levesque *et al.* also demonstrate the same features [53, 54], as shown in Fig. 4(a). The same pseudopotential holds at a higher T , viz., 0.8 eV as Z remains unchanged. The $T=0.8$ eV results are shown in Fig. 4(b).

Bonding features (e.g., the pre-peak in the $g(r)$ etc.) are unlikely to be captured by ion-sphere models as they limit the electron pileup at the pseudo-ions to within the ion-spheres, whereas the C-C bonding requires an increased density in the bonding regions *between the ions*. Starrett *et al.* [23] find no signs of C-C or C-H bonds using their code, for CH-plastic in a regime where DFT+MD studies show prepeaks due to C-C and C-H bonding.

The approximate correspondence of the successive peaks in $g(r)$ with the Friedel oscillations in the pair-potential given in panel (b) should be noted. The $g(r)$ is determined by the potential of mean force $V_m(r) = V_{ii}(r)/T + \text{Meanfield} + \text{Correlations}$, with $g(r) = \exp\{-V_m(r)\}$. The correspondence of the minima in $V_{ii}(r)$ and the maxima in $g(r)$ becomes less satisfactory for larger r/r_{ws} when the mean field and correlations kick in. These systems cannot be modeled by Thomas-Fermi or Yukawa-type potentials, a dominant paradigm even today. The DFT+MD simulations do not directly provide a pair-potential as N -ions with $N \sim 100$ are used in the simulation. The DFT+MD $g(r)$ can in principle be inverted to yield a pair-potential. The inversion of a $g(r)$ to a potential is not unique, and hence requires specify-

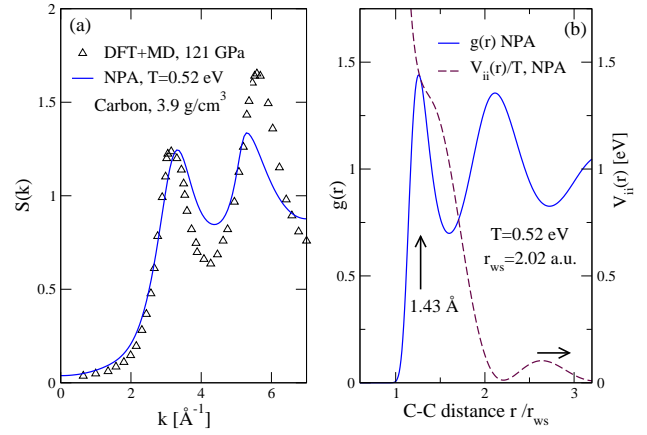


FIG. 5. (a) Comparison of the $S(k)$ of liquid carbon from the NPA with a DFT+MD (LDA) simulation [6] at 0.52 eV. (b) The corresponding NPA C-C potential in eV, together with the $g(r)$ from the NPA+HNC.

ing a *first-principles form* for $V_{ii}(r)$ and a $B(r)$, but it does not call for dynamic structure data [39, 46, 47]. One may also proceed as in Whitley *et al.* [5], who derived a C-C potential at 0.86 eV by force matching to DFT+MD. Their extracted V_{ii} (their Fig. 4(a)) is in good agreement with the NPA $V_{ii}(r)$, Fig. 3(b), but the Friedel oscillations are hard to capture using force-matching methods.

Applying NPA+HNC to a very low T case reveals its current limitations as well as the limitations of the second-order pair-potential given by Eq. 11 (see also Fig. 2). The DFT+MD simulations of Kraus *et al.* at $\rho=3.9$ g/cm³ and $T = 0.52$ eV provide a test case. This temperature is an order of magnitude smaller than that of the phase transition discussed in Sec. IV at $T = 7$ eV, and the density is nearly four times higher, with $\Gamma_{ii}=410$. As there is C-C bonding at such low T we use HNC (and not MHNC that employs a hard-sphere bridge correction). Figure 5 provides comparisons of NPA+HNC and DFT+MD at $T=0.52$ eV, i.e., 6000K. The $S(k)$ from NPA, Fig. 5(a) has peak positions within $\sim 5\%$ of the DFT+MD $S(k)$, but the second peak height is underestimated by as much as 19%. This error in the peak height may be due to: (a) shortcomings in the 2nd-order pair-potential (c.f., Fig. 2), and (b) the lack of a suitable bridge function for the C-C bonding peak in $g(r)$. These issues will be treated elsewhere.

B. Comparisons with PIMC.

In astrophysics, much higher temperatures and densities occur. The C-C association plays no role at the higher energy scales involved. Hence the hard-sphere LFA bridge function should be applicable. Judging by the value of Γ_{ii} , NPA+MHNC should be accurate. Hence a comparison can mutually validate NPA as well as PIMC calculations, and also validate the theory of Z used

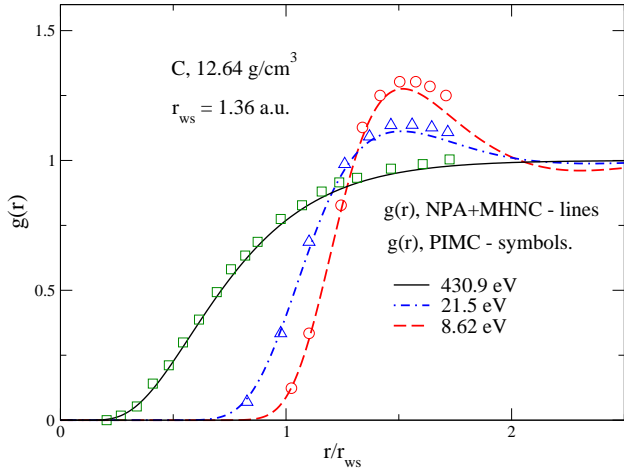


FIG. 6. The C-C pair-distribution functions $g(r)$ from the NPA (lines), and from PIMC/DFT from Ref. [10].

in NPA. We calculate the $g(r)$ of liquid-carbon, density 12.64 g/cm^3 , at $T = 8.62 \text{ eV}$ ($1 \times 10^5 \text{ K}$), 21.5 eV ($2.5 \times 10^5 \text{ K}$), and 430.9 eV ($5 \times 10^6 \text{ K}$) to compare with the PIMC and DFT+MD calculations of Driver and Militzer [10]. The mean ionization Z changes from 4.0 at low T , to 4.05 by $T = 100 \text{ eV}$, and reaches $Z=5.758$ by 430.9 eV , the highest T used by Driver *et al.*

Fig. 6 displays the $g(r)$ calculated using NPA+MHNC, and PIMC or DFT+MD. The symbols show the PIMC or DFT+MD $g(r)$ from Ref. [10] while the NPA+MHNC $g(r)$ are given as lines. The slight differences are due to limitations in the hard-sphere bridge functions used in the MHNC, and due to limitations in the calculations of Ref. [10] where only 24 carbon atoms have been used in DFT+MD simulations. As also noted by Starrett and Saumon (SS) [49] for $T=7.5 \times 10^5 \text{ K}$ (64.6 eV) given by Driver *et al.*, the PIMC $g(r)$ does not tend to unity for large r , but shows an error of $\sim 5\%$. Our $g(r)$ for $7.5 \times 10^5 \text{ K}$ is not shown in Fig. 6 to avoid overloading the figure. But it agrees closely with the $g(r)$ of SS (Ref. [49], Fig. 8) and the PIMC data to the expected extent. SS have not reported their $g(r)$ for lower T .

IV. MONOMER-DIMER PHASE-TRANSITIONS IN LOW-DENSITY LIQUID CARBON.

An ionization and temperature (or pressure) driven plasma phase transition was identified by Perrot and Dharma-wardana in WDM-aluminum via DFT [19]. Such plasma phase-transitions had been proposed by Norman *et al.* [55] and by others on general grounds. Simulations of such transitions in WDM have been reported by, e.g., Redmer *et al.* [56]. In a complex WDM liquid like carbon, the novel possibility of dimer-monomer transitions which are driven by “abrupt” changes in the ionization Z exists. Z must be 4 to have sp^3 , sp^2 or sp bonded species in carbon. WDMs are high in energy-

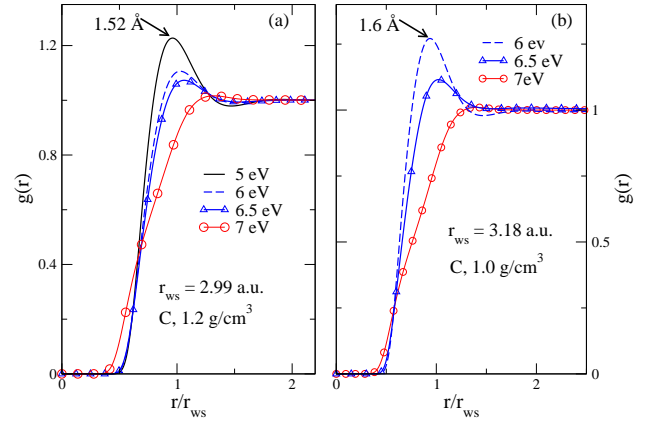


FIG. 7. (a) The evolution of the strongly correlated PDFs of liquid-carbon, 1.2 g/cm^3 for $T < 7 \text{ eV}$ across the (metal→semi-metal)+(liquid → vapour) transition at $\simeq 7 \text{ eV}$ to $g(r)$ of a weakly correlated vapour. The 1.52 \AA peak at 5 eV is a signature of the C-C bond. (b) The evolution of PDFs of liquid-carbon, 1.0 g/cm^3 across the transition. The

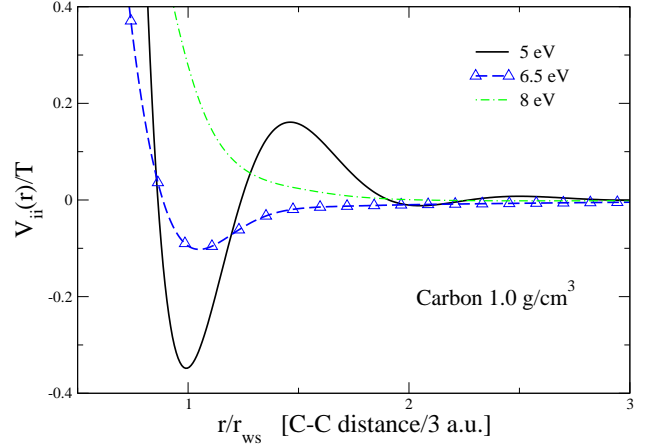


FIG. 8. Pairpotentials at $T=5, 6.5$ and 8 eV for carbon WDM at 1.0 g/cm^3 . At 5 eV $V_{ii}(r)$ is negative ($\sim 35\%$ of the thermal energy) at its minimum. The minimum occurs at the C-C bond distance of $\sim 3 \text{ a.u.}$ At this ρ, T carbon is a strongly correlated fluid. The potential at 6.5 eV yields the $g(r)$ shown in Fig. 7(b) at 6.5 eV . At 8.0 eV $V_{ii}(r)$ is repulsive and the fluid becomes an uncorrelated vapour.

density and Z -driven transitions are feasible.

Covalent bonding is enhanced at low densities and low temperatures. The covalent C-C distance ranges from 1.3 \AA to $\sim 1.6 \text{ \AA}$ (3.02 a.u.) or even 1.7 \AA depending on the coordination and screening by free-electrons. When the density drops to less than 1.05 g/cm^3 , the Wigner-Seitz radius r_{ws} is 3.02 a.u. , i.e., comparable to the C-C distance. We study liquid-carbon at the density $1.0\text{-}1.4 \text{ g/cm}^3$ in the context of changes in the mean ionization Z with temperature, and the disruption of the ‘dimers’ in favor of the monomers.

Fig. 1 indicates sharp *downward* changes in Z , both

for C at 2.0 g/cm^3 and 1.0 g/cm^3 . Unlike a rise in Z caused by shell ionization, downward drops are indicative of metal-semimetal transitions. Furthermore, the bound-electron core of the carbon atom remains compactly within the WS-sphere, and hence there is no ambiguity in defining $Z = Z_n - n_b$ (this is further discussed in the appendix in the context of the transition). Even in the transition region the Friedel sum rule on Z , the f -sum rule, and the conditions for the validity of the linear-response construction of pseudopotentials (which depend on Z being correct) [35] are satisfied to better than 93%) by the NPA-LDA calculation. Hence the drop in \bar{n} and the discontinuity in Z at 7 eV should be observable in the EOS, $g(r)$, conductivity, compression etc., as further discussed below.

In the case of carbon at $\sim 1.0 \text{ g/cm}^3$, an average ‘dimer’ fluid which has dynamical long-range order (Fig. 2) converts to a monomer fluid. It is simultaneously a *metal*→*semi-metal*, *liquid*→*vapour* transition, with a sharp drop in Z at 7 eV for carbon at 1 g/cm^3 . The properties show “hysteresis” typical of such transitions. Since $\Gamma_{ii} = Z^2/(r_{ws}T)$ for this case is $\simeq 19$, NPA+HNC methods are eminently applicable here.

In Fig. 7 the $g(r)$ for two densities at the transition are displayed for $5 \leq T \leq 7 \text{ eV}$. At $T=5 \text{ eV}$ the mean charge Z is 4, while the C-C distance as given by the 1st peak position in $g(r)$, panel (a), is slightly larger than r_{ws} . But it qualifies ($\sim 1.52 \text{ \AA}$) for a typical C-C bond with a bond length of 1.4-1.7 \AA . The peak weakens and the average bond length increases slightly as the temperature is raised, as seen from the peak positions of the $g(r)$ at $T=6 \text{ eV}$ and 6.5 eV . Strikingly, at 7 eV all C-C correlations are abruptly lost, and we have a mono-atomic carbon fluid with a *reduced* ionization $Z \simeq 2.8$. There is a gain in entropy in the dimer → monomer transition, i.e., a complex liquid with transient C-C bonding transitioning to a random-monomer liquid, as in a liquid→vapor transition. This transition clearly has analogies to the vaporization of water where transient hydrogen bonds in liquid water break down cooperatively to produced essentially water monomers in the vapour phase. Hydrogen bonding in liquid-water involves the lone-pair electrons in the oxygen, and its energy scale is much smaller ($\sim 5 \text{ kcal/mole}$) than the transient C-C covalent bond relevant to the liquid-carbon phase transition.

The evolution of the liquid from a strongly correlated C-C bonded fluid to a disordered atomic vapour is manifested in the $V_{ii}(r)$ shown in Fig. 8. Given the negative pair-potential at 5 eV and below, persistent C-C bonding occurs and the HNC equations do not easily converge. However, NPA+MD can be used for such cases.

Fig. 9 explores the critical region in ρ ($1.0\text{-}1.4 \text{ g/cm}^3$) and T ($5\text{-}10 \text{ eV}$). The transition occurs near $T = 7 \text{ eV}$ with ρ below $\sim 1.4 \text{ g/cm}^3$. At 1.4 g/cm^3 Z is 4, with no transition. For $\rho < 1.4$, Z dips to ~ 3 near $T > 7 \text{ eV}$. The compressibility κ as reflected in $S(0) = \rho T \kappa$, Fig. 9(a), and the resistivity R , Fig. 9(b), show discontinuities near 7 eV typical of a transition.

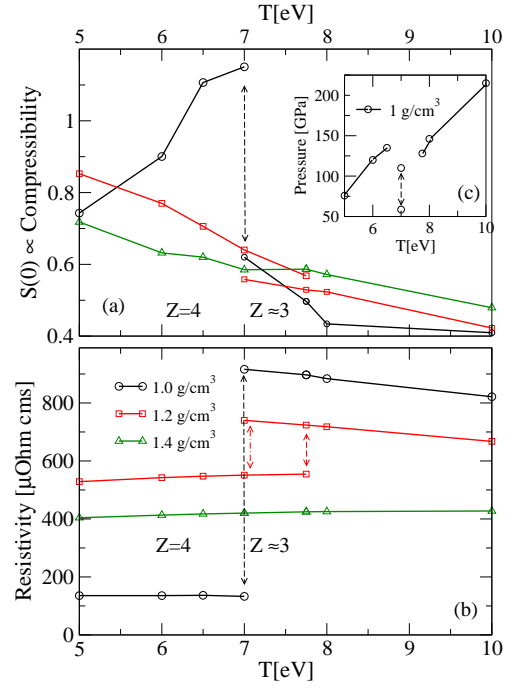


FIG. 9. Vertical arrows connect two possible WDM-carbon fluids. (a) The variation of the compressibility of carbon for $1.0 \leq \rho \leq 1.4 \text{ g/cm}^3$ density and $5 \leq T \leq 10$. (b) Variation of the resistivity. (c) Variation of P with T , $\rho = 1.0 \text{ g/cm}^3$.

The pseudopotential $U_{ei}(k)$ and the structure factor $S(k)$ for carbon obtained from the NPA+HNC calculation are used in the Ziman formula (used in the form of Eq. 31, Ref. [19]) to calculate the resistivity displayed here. The variation of the pressure with T , at $\rho = 1.0 \text{ g/cm}^3$ is shown in Fig. 9(c) and confirms the transition. Furthermore, for $\rho = 1.2 \text{ g/cm}^3$ the super-heating of the $Z = 4$ fluid to 7.75 eV, and the supercooling of the $Z \sim 3$ mono-ionic form from 7.75 to 7 eV give rise to two Kohn-Sham solutions. Thus at 1.0 g/cm^3 a narrow metastable ‘two-solution’ region around 7 eV exists.

The NPA model accommodates a pseudo-binary mixture of fluids (e.g., monomer and average dimer) but cannot be pushed too far into lower ρ, T since it treats the fluid as a single ‘average’ species and its *transient* pairs. For $6.5 \text{ eV} < T < 7.5 \text{ eV}$, the value of Z moves from 4 to approximately three. Since Z is close to an integer value, the single-species AA model with LDA-XC is adequate. This is not the case near $T \geq 20 \text{ eV}$ where a multi-species C^{+Z} fluid and XC-functionals beyond LDA are needed.

At lower densities and lower T , persistent molecular forms begin to dominate while monomers vanish. Hence a more sophisticated ‘neutral-pseudo-molecule’ model becomes necessary for applications to low- T low-density complex fluids with hardly any monomers. However, carbon and other low- Z_n elements of the periodic table do not usually involve interactions of bound electron states which extend outside their WS-spheres in forming quasi-bound states as in, say, gold. Hence many interesting

low- Z_n elements and their mixtures are likely to show phase transitions similar to those of carbon.

Conclusion. Calculations are presented to validate the NPA model for complex liquids with transient covalent bonding, using the example of carbon. The method recovers heavy DFT+MD and PIMC simulation results with good accuracy from simple computations. The NPA provides an unequivocal value for the mean-ionization Z , bound and free spectra, phase shifts, pair-potentials, and structure factors needed in WDM calculations within a single theory. In regard to discontinuities in Z , the need for XC-models which include GW and self-interaction corrections, and the need to use a mixture of ions if Z is close to a half-integer value, are emphasized.

Application to low-density liquid carbon has revealed a novel *a metal-semi-metal* transition that occurs simultaneously with a *liquid-vapor* transition in the WDM regime. Such transitions in carbon, (and most likely in CH plastic used in ICF-ablators), and in other low- Z_n elements may be of immediate importance in planetary physics, ICF ablator physics, and in carbon technologies.

Appendix: The electronic structure of Carbon at 6 eV to 10 eV, and the Z discontinuity at ~ 7 eV.

The mean electron density/ion, Z , is defined in the NPA model as equal to $Z_b = Z_n - n_b$, where $Z_n = 6$, self-consistently agreeing with Z_{cn} , Eq. 5 and with the Friedel sum $Z_f - Z = 0$. The bound electrons totaling n_b should be compactly contained in the WS-sphere of carbon. That is, if the outermost bound-electron shell has a mean radius $\langle r \rangle$ distinctly less than r_{ws} , there is no ambiguity in setting $Z = Z_b$. In fact Z is the usual chemical valance of the atom at normal density and pressure, but becomes non-integral for finite- T where DFT-level occupations are Fermi factors, f_{nl} . The chemical potential used in f_{nl} is μ^0 , the value for a *homogeneous non-interacting* electron gas, consistent with DFT. The T, \bar{n} dependence in f_{nl}, ϵ_{nl} and in the finite- T phase shifts link Z_{cn}, Z_b, Z_F to thermodynamics *via* the Kohn-Sham-Mermin formalism [19]. The Kohn-Sham level structure and Z at a carbon nucleus for liquid-carbon at 1.0 g/cm³ at 6 eV-10 eV are given in Table I. The rapid change in Z near 7 eV is evident in Fig. 1. The Kohn-Sham equation

at $T=7$ eV has two solutions, one with $Z=4$ and zero occupation in the $n = 2$ state, and another with $Z = 2.78$ and having a $n=2$ state with an occupation of ~ 0.71 and a mean radius $\langle r \rangle = 1.995$ a.u. $Z=2.78$ is clearly a $Z = 3$ state corrupted by the lack of self-interaction corrections in the F_{xc}^{ec} -LDA form. The bound state is wholly inside the carbon Wigner-Seitz sphere of radius 3.18 a.u.

Whitley *et al.* [5] used a constant mean ionization $Z=3.2$ (for the range of their study) for carbon, together with Yukawa screening to model the potentials fitted to their DFT+MD calculations at 0.86eV *via* a force-field analysis. Their PDFs show features due to a C-C bond,

TABLE I. Kohn-Sham energies ϵ_{nl} (a.u.) and occupations for carbon at 1.0 g/cm³. Here $2f_{nl}$ includes spin. There are two solutions with two values of Z at $T=7$ eV. The bound-states with radii $\langle r \rangle$ in a.u., are well inside the WS sphere, $r_{ws} = 3.18$ a.u. The Friedel sum value of Z from phase shifts, the charge-neutrality estimate $Z_{cn} = (4\pi/3)\bar{n}r_{ws}^3$ and $Z_b = 6 - n_b$ agree to better than $\sim 93\%$ even at the phase transition. When one value of Z is given, agreement is $\sim 100\%$.

T eV	$-\epsilon_{nl}$	$2f_{nl}$	$\langle r \rangle$	Z_{cn} $Z = 6 - n_b$
6.0	1s , 19.181	2.00	0.269	4.0
7.0 (state 1)	1s , 18.647	2.00	0.273	4.0
7.0 (state 2)	1s , 18.932	2.00	0.273	2.78
	2s , 0.1256	1.42	1.995	2.58
8.0	1s , 19.793	2.00	0.267	2.81
	2s , 0.1709	1.33	1.854	2.67
10.0	1s , 20.073	2.0	0.266	2.94
	2s , 0.2196	1.15	1.757	2.85

as also recognized by them. The existence of such bonds implies a value of $Z = 4$ which is in fact compatible with their data. The Thomas-Fermi ionization Z_{tf} used in the conductivity model of Lee and More [57] (also in the Quotidien equation of state (QEOS) [58]) is displayed in Fig. 1(a) together with the NPA Z for liquid carbon in the range 1.0-3.7 g/cm³. Thomas-Fermi (TF) theory does not have shell structure, and it is also not suitable for light elements at normal and low densities.

-
- [1] G. Galli, R. M. Martin, R. Car, and M. Parrinello, Phys. Phys. Rev. Lett. **63**, 988 (1989).
[2] J. N. Glosli and F. H. Ree, Phys. Rev. Lett. **82**, 4659 (1999).
[3] L. M. Ghiringhelli, Jan H. Los, A. Fasolino, Phys. Rev. B **72**, 214103, (2005).
[4] M. W. C. Dharma-wardana and F. Perrot, Phys. Rev. Lett., **65**, 76 (1990).
[5] H. D. Whitley, D. M. Sanchez, S. Hamell, *et al.*, Contrib. Plasma Phys. **55**, 390 (2015).
[6] D. Kraus, J. Vorberger, D. O. Gericke, *et al.* Phys. Rev. Lett. **111**, 255501 (2013).
[7] Sebastian Hamel, Lorin X. Benedict, Peter M. Celliers *et al.* Phys. Rev. B **86**, 094113 (2012).
[8] W. B. Hubbard, W. J. Nellis, A. C. Mitchell, *et al.*, Science **253**, 648 (1991).
[9] B. L. Sherman, H. F. Wilson, D. Weeraratne, and B. Militzer, Phys. Rev. B **86**, 224113 (2012).
[10] K. P. Driver and B. Militzer, Phys. Rev. Lett. **108**, 115502 (2012).

- [11] J. D. Lindl, P. Amendt, R. L. Berger, *et al.*, Phys. Plasmas **11**, 339 (2004).
- [12] L. X. Benedict, K. P. Driver, S. Hamel, *et al.* Phys. Rev. B **89** 224109 (2014).
- [13] A. I. Savvatimskiy, Journal of Physics: Condensed Matter **20**, 114112 (2008).
- [14] J. H. Los and A. Fasolino, Phys. Rev. B **68**, 024107 (2003).
- [15] J. H. Los, Luca M. Ghiringhelli, Evert Jan Meijer, and A. Fasolino, Phys. Rev. B **72**, 214102 (2005).
- [16] M. W. C. Dharma-wardana, Contrib. Plasma Phys. **55**, No.2-3, 79-81 (2015).
- [17] F. Perrot, Phys. Rev. E **47**, 570 (1993).
- [18] F. Perrot, M. W. C. Dharma-wardana, and John Benage, Phys. Rev. E **65**, 046414 (2002)
- [19] F. Perrot and M.W.C. Dharma-wardana, Phys. Rev. E. **52**, 5352 (1995).
- [20] Michael S. Murillo, Jon Weisheit, Stephanie B. Hansen, and M. W. C. Dharma-wardana, Phys. Rev. E **87**, 063113 (2013).
- [21] G. Gregori, *et al.*, Contrib. Plasma Phys. **45**, 284 (2005)
- [22] B. Wilson, V. Sonnad, P. Sterne, J. Quant. Spectrosc. Radiat. Transf. **99** 658-679 (2006).
- [23] C. E. Starrett, D. Saumon, J. Daligault, and S. Hamel Phys. Rev. E **90**, 033110 (2014)
- [24] T. Blenski, R. Piron, C. Caizergues and Bogdan Cichocki, High Energy Density Phys. **9**, 687-695 (2013)
- [25] R. Piron and T. Blenski, Phys. Rev. E **83**, 026403 (2011)
- [26] P.A. Sterne S.B. Hansen, B.G. Wilson, W.A. Isaacs, HEDP, **3**, 278 (2007)
- [27] M. W. C. Dharma-wardana and F. Perrot, Phys. Rev. A **26**, 2096 (1982)
- [28] E. K. U. Gross, and R. M. Dreizler, *Density Functional Theory*, NATO ASI series, **337**, 625 Plenum Press, New York (1993).
- [29] J. Chihara, J. Phys. F: Met. Phys. **17** 295 (1987)
- [30] F. Perrot, Y. Furutani and M.W.C. Dharma-wardana, Phys. Rev. A **41**, 1096-1104 (1990)
- [31] L. Dagens, J. Phys. (Paris) **36**, 521 (1975).
- [32] L. Harbour, M. W. C. Dharma-wardana, D. D. Klug, L. J. Lewis, Contr. Plasma Phys. **55**, 144-151 (2015)
- [33] S. H. Glenzer and Ronald Redmer, Rev. Mod. Phys. **81** 1625 (2009)
- [34] F. Perrot and M. W. C. Dharma-wardana, Phys. Rev. A **29**, 1378 (1984)
- [35] M. W. C. Dharma-wardana, Phys. Rev. E **86**, 036407 (2012).
- [36] L. Harbour, M. W. C. Dharma-wardana, D. D. Klug and L. J. Lewis, Physical Review E **94**, 053211, (2016)
- [37] F. Perrot and M. W. C. Dharma-wardana, Phys. Rev. B **62**, 16536 (2000); *Erratum:* **67**, 79901 (2003); arXiv:1602.04734 (2016).
- [38] F. Lado, S. M. Foiles, and N. W. Ashcroft, Phys. Rev. A **28**, 2374 (1983).
- [39] H. C. Chen and S. K. Lai, Phys. Rev. A **45**, 3831 (1992).
- [40] M. W. C. Dharma-wardana, *A physicist's view of matter and mind*, Ch 8-9, World Scientific, New Jersey (2013)
- [41] A. Heslot, Phys. Rev. D **31**, 1341 (1985)
- [42] H. Ehrenreich, H. R. Philipp, AND B. Segal, Phys. Rev. **132**, 1918 (1963)
- [43] N. E. Christensen and B. O. Seraphin, Phys. Rev. B **4**, 3321 (1971).
- [44] M. L. Thèye, Phys. Rev. B **2**, 3060 (1970)
- [45] M. W. C. Dharma-wardana, Phys. Rev. E **93**, 063205 (2016); arXiv:1602.04734 (2016).
- [46] N. H. March, Can. J. of Phys., **65**, 219-240, (1987).
- [47] M.W.C. Dharma-wardana and G.C. Aers, Phys. Rev. B. **28**, 1701 (1983).
- [48] W. Kohn and C. majumdar, Phys. Rev. **138**, A1617 (1965)
- [49] C. E. Starrett and D. Saumon, Phys. Rev. E **87**, 013104 (2013)
- [50] F. Perrot and M. Rasolt, Phys. Rev. B **27**, 3273 (1983)
- [51] Alfredo A. Correa, Stanimir A. Bonev, and Giulia Galli, PNAS, **103**, 1204 (2006)
- [52] S. Strassler and C. Kittel, Phys. Rev. **139**, A758 (1965).
- [53] Dharma-wardana, M. W. C. and Aers, G. C., Phys. Rev. Lett.**56**, 1211 (1986)
- [54] D. Levesque, J. J. Weis, and L. Reatto Phys. Rev. Lett. **54**, 451 (1985).
- [55] G. E. Norman and A. N. Starostin, High Temp. **6**, 394 (1968).
- [56] W. Lorenzen, B. Holst, and R. Redmer, Phys. Rev. B **82**, 195107 (2010).
- [57] Y. T. Lee and R. M. More, Phys. Fluids **27**, 1273 (1984).
- [58] R.M. More, K.H. Warren, D.A. Young, and G.B. Zimmerman, Phys. Fluids **31**, 3059 (1988).